11th Australasian Fluid Mechanics Conference
University of Tasmania, Hobart, Australia
14-18 December 1992

CONVECTION OVER TOPOGRAPHY IN ROTATING FLUIDS

Scott A. CONDIE[1] and Peter B. RHINES[2]

[1]Research School of Earth Sciences, Australian National University, Canberra, ACT 2601, AUSTRALIA

[2]School of Oceanography WB-10, University of Washington, Seattle WA 98195, USA

ABSTRACT

When a rotating fluid over sloping topography is uniformly cooled from above, convection cells aligned with isobaths develop. We refer to these cells as *topographic Hadley Cells*. Sinking occurs in small cyclonic vortices situated in relatively shallow regions. This is balanced by slower upwelling in adjacent deeper regions. The cross-isobath motions which connect the upwelling and downwelling are accelerated in the along isobath direction by Coriolis forces. The cells are therefore characterized by strong isobathic jets which are found to be unstable. For anti-clockwise rotation the surface jets keep the shallows to their left when looking in the direction of flow. A linear inviscid theory is presented which predicts the surface velocity, density distribution and size of the cells. Laboratory experiments provide preliminary support for the theory. Topographic Hadley cells may be an important mode of heat (or salt) transfer in continental shelf and slope seas where surface cooling (or evaporation) drives convection.

INTRODUCTION

If a fluid of varying depth is uniformly cooled from above, the coldest fluid will be produced in the most shallow regions due to the smaller heat capacity per unit area. This can result in the development of convection cells characterized by downwelling in shallows balanced by upwelling in deeper regions. In this way heat is transfered from deep to shallow regions. If the fluid is also rotating, the horizontal motions within the cell will be accelerated by Coriolis forces. This is illustrated schematically in Fig.1. As relatively warm fluid nears the free surface and begins to move toward the shallows, it will be accelerated to the right (anti-clockwise rotation), thus forming a zonal along isobath jet which keeps the shallows to its left. The bottom flow will similarly form a jet in the opposite direction, co-directional with topographic Rossby waves. These motions will not necessarily be purely baroclinic, since Ekman friction may significantly modify the bottom flow.

The convection cells can be readily reproduced in the laboratory. Fig.2 shows a rotating hemispherical bowl, containing water cooled at the free surface and insulated below. The surface flow is visualized by a streak photograph of floating aluminium powder. The flow is dominated by highly unstable anticyclonic (clockwise) jets, separated by rings of small cyclonic (anti-clockwise) vortices. The vortices form the downwelling component of the convection cells, carrying cooled surface water downward in spiralling motions to the bottom. These structures are closely related to those observed in rotating Bénard convection experiments over a flat bottom (Boubnov and Golitsyn 1986, Chen et al. 1989, Fernando et al. 1991). Without topography, downwelling in cyclonic vortices is surrounded by anticyclonic upwelling motions. However, with the addition of topography as in Fig.2, upwelling occurs in adjacent deeper regions where it generates the zonal jets.

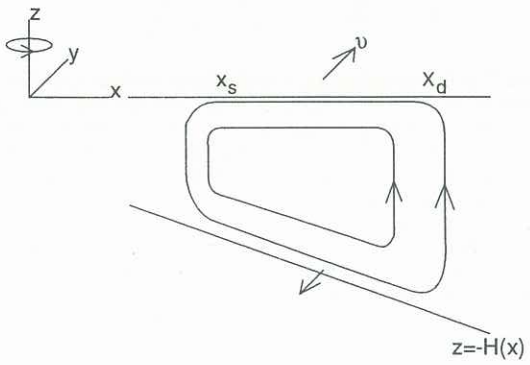

Fig.1. A schematic representation of the convection cell.

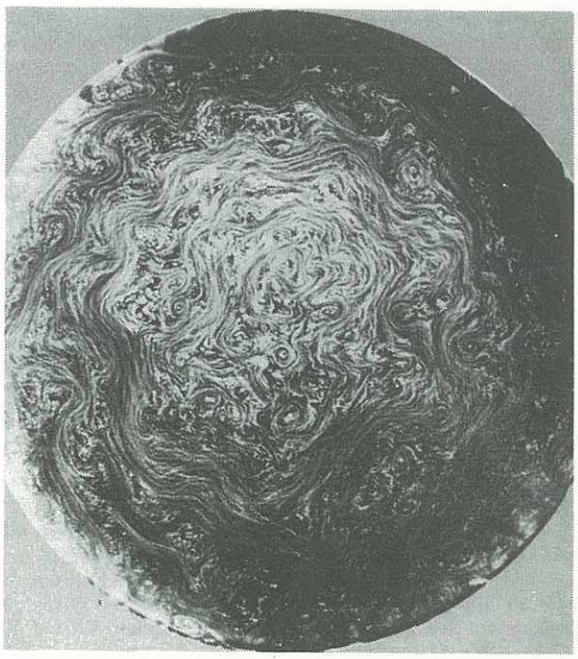

Fig.2. Surface flow in a bowl of water cooled from above. The bowl was 46cm in diameter at the free surface and the maximum fluid depth was 11cm. The rotation rate corresponded to $f = 1.4s^{-1}$ and the temperature difference between the air and water was 12°C.

There exists a close dynamical analogy between the formation of zonal jets over topography and the formation of the jet stream by the atmospheric Hadley cell (Held and Hou 1980). For this reason we refer to the convection cells as *topographic Hadley cells.*

CONDITIONS FOR CELL GENERATION

To understand the conditions under which topographic Hadley cells might develop, consider again the system shown in Fig.1. Assuming that gradients along isobaths are negligible, the heat equation in the shallow region (denoted by subscript s) can be written

$$\frac{\partial T_s}{\partial t} + u\frac{\partial T_s}{\partial x} = \kappa\frac{\partial^2 T_s}{\partial x^2} - \frac{Q_s}{\rho c_p H_s}, \qquad (1)$$

and similarly in the deeper region (denoted by subscript d)

$$\frac{\partial T_d}{\partial t} + u\frac{\partial T_d}{\partial x} = \kappa\frac{\partial^2 T_d}{\partial x^2} - \frac{Q_d}{\rho c_p H_d}. \qquad (2)$$

Here T is the temperature, u is the cross isobath (x) velocity component, H is the depth, Q is the surface heat flux, ρ is the density and c_p is the specific heat. The horizontal transport associated with turbulent processes, such as convective vortices, is conveniently characterized by a constant diffusivity κ.

If the fluid is cooling uniformly, such that the horizontal temperature gradients are steady, then $\partial T_s/\partial t = \partial T_d/\partial t$ and (1) and (2) can be combined into a single equation. If there is no Hadley cell, then the advective terms are zero (u = 0) and we are left with a balance between surface cooling and horizontal diffusion:

$$\frac{Q_d}{H_d} - \frac{Q_s}{H_s} = \rho c_p \kappa\frac{\partial^2}{\partial x^2}(T_d - T_s). \qquad (3)$$

However, if the heat flux term exceeds the diffusion term, then the advective term must make a contribution through the formation of a Hadley cell. For uniform surface flux ($Q=Q_s=Q_d$), the condition for the formation of a cell can therefore be written in scaled form as

$$Q > \frac{\rho c_p \kappa \bar{H}^2 \Delta T}{\beta \Delta x^3}. \qquad (4)$$

Here $\bar{H}$ is the mean depth scale, $\Delta T = T_d - T_s$ is the temperature drop across the cell, $\beta = (H_d - H_s)/\Delta x$ is the slope of the topography and $\Delta x = x_d - x_s$ is the width of the cell. Relation (4) has little predictive power since the use of simple diffusion may not be appropriate and κ is in any case poorly constrained. However, the functional form of (4) is valid and can provide insight into the influence of the various parameters. In particular, a cell is unlikely to form in a very deep region or where the slope is very gentle. In both cases significant horizontal temperature gradients cannot develop from uniform surface cooling.

THEORY

The dynamics of the convective vortices which form the downwelling arm of the topographic Hadley cells are turbulent and non-hydrostatic, making theoretical progress beyond linear stability analysis particularly difficult (Nakagawa and Frenzen 1955, Chandrasekhar 1961). In contrast, the jet regions are less thermodynamically active and are likely to be near hydrostatic balance. They may also be assumed to be dominated by a geostrophic balance in the cross-stream direction. These assumptions will now be utilized in a linear inviscid theory which predicts the free surface velocity distribution, the depth averaged density distribution and the size of the cell.

Consider again a cell like that in Fig.1 with no isobathic gradients. The cross isobath (x) momentum balance is geostrophic,

$$-f\upsilon = -\frac{1}{\rho_o}\frac{\partial p}{\partial x}, \qquad (5)$$

while the vertical (z) momentum equation for hydrostatic Bousinesq flow is

$$0 = -\frac{1}{\rho}\frac{\partial p}{\partial z} - g. \qquad (6)$$

Here, $\upsilon(x,z)$ is the along isobath velocity, $p(x,z)$ is the pressure, ρ_o is the mean density, g is the gravitational acceleration and f is the Coriolis parameter. Our third assumption is that the surface flow is inviscid so that the angular momentum per unit mass,

$$M = \tfrac{1}{2} f x^2 + \upsilon x, \qquad (7)$$

is conserved.

If the cell extends across isobaths from $x = x_s$ to $x = x_d$, then (7) implies immediately that the surface velocity is

$$\upsilon(x,0) = \frac{f x_d}{2}\left(\frac{x_d}{x} - \frac{x}{x_d}\right), \qquad (8)$$

while bottom friction should ensure that

$$\upsilon(x,-H) \ll \upsilon(x,0). \qquad (9)$$

The surface velocity is plotted as a function of position in Fig.3. Warm fluid surfaces with zero horizontal velocity at $x = x_d$, then accelerates zonally as x decreases. It finally sinks at $x = x_s$ where the maximum velocity is

$$\upsilon(x_s,0) = f\Delta x\left(1 + \frac{\Delta x}{2x_s}\right). \qquad (10)$$

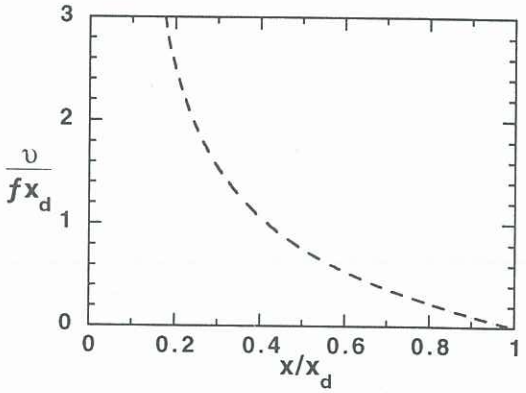

Fig.3. Non-dimensional zonal velocity as a function of cross cell coordinate. The fluid depth increases with increasing x.

Eliminating the pressure term from (5) and (6) to produce the thermal wind equation, then integrating from the bottom $z = -H(x)$ to the free surface $z = 0$, yields

$$f\{\upsilon(x,0) - \upsilon(x,-H)\} = -g\bar{H}\frac{\partial \sigma}{\partial x}, \qquad (11)$$

where $\bar{H}$ is the mean depth of the cell and the non-dimensional depth averaged density distribution is defined by

$$\sigma(x) = \frac{1}{\rho_o \bar{H}}\int_{-H}^{0} \rho dz, \qquad (12)$$

Since ρ_o is the mean density of the cell, we can also write

$$\int_{x_s}^{x_d} \sigma \, dx = \Delta x. \tag{13}$$

Utilising the boundary conditions (8) and (9) in relation (11), then integrating from x to x_d yields an expression for the depth averaged density distribution,

$$\sigma = \sigma_d + \frac{\chi}{4}\left\{\frac{x^2}{x_d^2} - 2\,\ln\left(\frac{x}{x_d}\right) - 1\right\}, \tag{14}$$

where $\sigma_d = \sigma(x_d)$ and $\chi = f^2 x_d^2/g\bar{H}$. The density distribution is plotted as a function of position in Fig.4. The density increases with decreasing x until sinking occurs at a critical density $\sigma_s = \sigma(x_s)$.

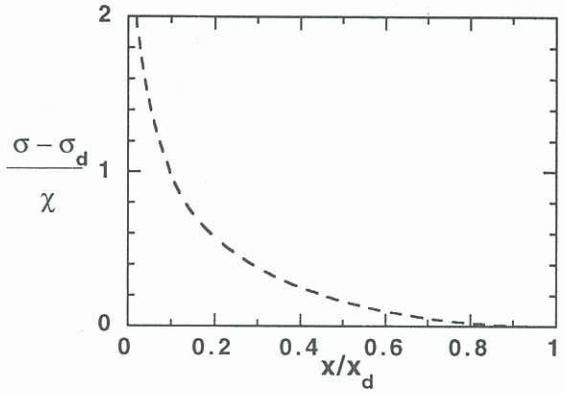

Fig.4. Depth averaged density anomaly as a function of cross cell coordinate. The fluid depth increases with increasing x.

It is now convenient to introduce a non-dimensional coordinate $x^* = x/x_d$. Equations (13) and (14) can then be rewritten in the respective forms

$$\int_{x_s^*}^{1} \sigma \, dx^* = \Delta x^*, \tag{15}$$

and

$$\sigma = \sigma_d + \frac{\chi}{4}\left\{x^{*2} - 2\,\ln(x^*) - 1\right\}, \tag{16}$$

where $x_s^* = x_s/x_d$ and $\Delta x^* = \Delta x/x_d$. Substituting (16) into (15) yields

$$\sigma_d = 1 + \frac{\chi}{4(1-x_s^*)}\left\{\frac{2}{3}x_s^{*3} - 2x_s^*\ln(x_s^*) + x_s^* - \frac{4}{3}\right\}, \tag{17}$$

which when substituted back into (16) gives,

$$\sigma = 1 + \frac{\chi}{4}\left\{x^{*2} - 2\,\ln(x^*) - 1 + \frac{1}{(1-x_s^*)}\left[\frac{2}{3}x_s^{*3} - 2x_s^*\ln(x_s^*) + x_s^* - \frac{4}{3}\right]\right\}. \tag{18}$$

If the location of both sides of the cell are known, then (18) can be used to calculate the density distribution.

If the density change across the cell is defined as $\Delta\sigma = \sigma_s - \sigma_d$, then equation (16) gives,

$$\Delta\sigma = \frac{\chi}{4}\left\{\Delta x^{*2} - 2\,\ln(1 - \Delta x^*) - 2\Delta x^*\right\}, \tag{19}$$

where we have substituted $x_s^* = 1 - \Delta x^*$. The power series expansion

$$\ln(1 - \Delta x^*) = -\Delta x^*\left[1 + \tfrac{1}{2}\Delta x^* + O(\Delta x^{*2})\right], \tag{20}$$

when substituted into (19) yields

$$\Delta x^* = \left(\frac{2\Delta\sigma}{\chi}\right)^{1/2} \tag{21}$$

to $O(\Delta x^{*2})$. In dimensional form, (21) corresponds to a cell width of

$$\Delta x = 2^{1/2}R, \tag{22}$$

where

$$R = \frac{(g\Delta\sigma\bar{H})^{1/2}}{f} \tag{23}$$

is an internal deformation radius based on the depth averaged horizontal density change and average depth of the cell. Note that the width of the cell depends on the detailed topography only through $\Delta\sigma$ and $\bar{H}$.

EXPERIMENTS

A preliminary series of laboratory experiments have provided an initial test of the theory. A shallow bowl of 80cm diameter (larger than that in Fig.2) was filled to a depth of 15cm with water warmer than the laboratory environment by $\Delta T = 15°C$. The outside surface of the rotating bowl was insulated, while cooling was allowed at the free surface. The flow was visualized using aluminium powder and still photographs similar to that in Fig.2 were recorded. This method does not provide accurate velocities, but did reveal cell widths and demonstrated qualitatively that the jet velocity increases towards the shallows as suggested by relation (8).

The width of the zonal jets were measured at eight evenly spaced locations along their circumference. The mean jet width and its standard deviation is plotted for a range of rotation rates in Fig.5. The cell width is non-dimensionalized by R, which was calculated using $\Delta\sigma = \alpha\Delta T$, where α is the coefficient of thermal expansion. It seems reasonable to assume that $\Delta\sigma$ from the theory will scale with this quantity, although this point is under further investigation. The plot indicates that the cell width scales with the deformation radius in accordance with (22) over most of the parameter range. The only exception is an experiment in which the deformation radius was comparable to the radius of the bowl L_o. In this case $\Delta x^* = O(1)$ and higher order terms in (21) cannot be neglected. From a physical viewpoint, the width of the cell was constrained by the finite size of the bowl.

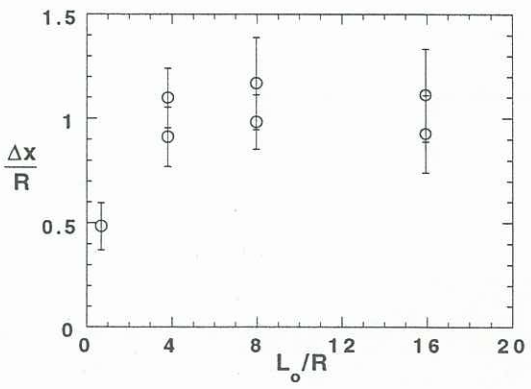

Fig.5. Non-dimensional cell width as a function of basin radius (non-dimensionalized by R).

Fig.2 also demonstrates that the zonal jets could be highly unstable. Waves were first evident when $R \sim L_o$ and became progressively more nonlinear as R decreased. The wavelengths of these features were often difficult to measure because of nonlinear interactions, but like the current width appeared to scale with the deformation radius. When $R \ll L_o$, all measurable wavelengths lay in the range $(1.4\pm0.3)R$. This value decreased to $(0.7\pm0.1)R$ when $L_o/R = 0.7$, a similar reduction to that of the current width.

In a second series of experiments, azimuthal velocities were measured with a laser Doppler velocimeter (LDV). These were conducted in the smaller bowl shown in Fig.2. The experiment differed from those described above in that the surface was cooled by a cold water bath, separated from the flow by a thin plastic film which was transparent to the LDV. Submerging the head of the LDV in the cold bath, while focusing it in the experimental flow, avoided problems associated with focusing through a free surface.

Fig.6 shows examples of instantaneous and mean azimuthal velocity distributions across the radius of the bowl (3cm below the rigid surface film). The smoothed instantaneous signal (Fig.6a) corresponds to a single continuous transect with a spatial resolution of approximately 0.01R. The mean values (Fig.6b) were calculated from stationary readings taken over a 200s period with a maximum sampling frequency of 15 per second. The error bars on these values correspond to one standard deviation in the natural variation of the signal.

The instantaneous signal is chaotic, however, there is distinct structure evident on the deformation radius scale. Another transect higher in the water column (not shown) suggests that this structure diminished with depth. The range of velocities also decreased with depth, although the maximum speed 1.5cm below the lid was still much less than fR. There is no clear net transport evident in Fig.6a, suggesting that much of the signal is generated by turbulent vortices. In contrast, the mean field in Fig.6b reveals significant anticyclonic (clockwise) transport at this depth. As a result of the radial meandering of the jets, the mean velocity tends to be broadly distributed over the bowl radius.

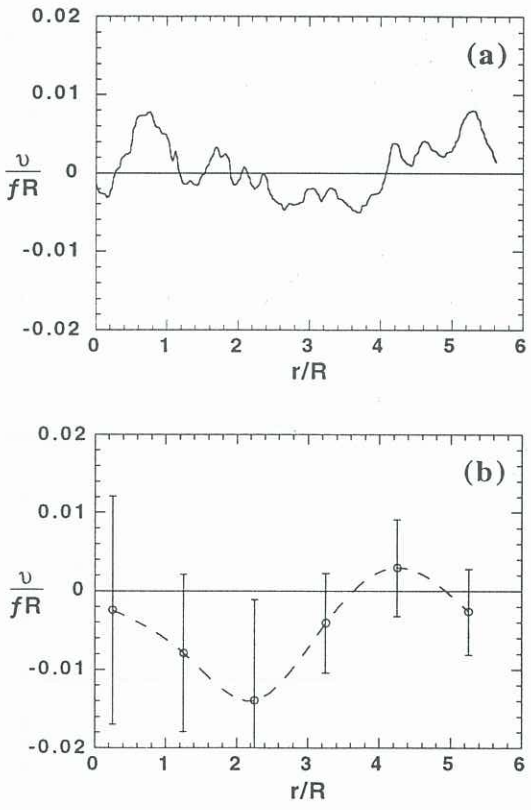

Fig.6. Non-dimensional radial distribution of azimuthal velocity. Measurements were taken 3cm below the surface in a flow with a maximum depth of 14cm. The rotation rate was $f = 1.0s^{-1}$ and the temperature difference between the cold bath and working fluid was around $\Delta T = 7°C$. (a) Instantaneous velocity distribution after simple boxcar smoothing. (b) Mean velocities at six different radii fitted by a cubic spline. The error bars represent one standard deviation in the measured velocities.

The experiments appear to provide preliminary support for the theoretical arguments and reveal additional features not included in the simple theory. Further experiments involving detailed temperature and surface velocity measurements should provide more definitive tests.

DISCUSSION

Topographic Hadley cells have been analysed under assumptions of hydrostatic flow, geostrophy and inviscid surface flow which conserves angular momentum. This yielded cell characteristics such as the surface velocity field, depth integrated density field and cell width. Preliminary laboratory experiments confirm that the cell width scales with the internal deformation radius and further show that the wavelength of jet instabilities obey a similar scaling.

To extend the present theory to include frictional effects would require a full numerical solution. However, there are a number of logical consequences associated with increasing the fluid viscosity. Firstly, the laboratory experiments demonstrated that the zonal jets are very unstable and we would expect that friction may significantly modify the growth rate of these waves. Secondly, friction would tend to break the angular momentum constraint, thereby reducing zonal jet velocities and allowing the cell width to increase beyond the inviscid values. This type of behaviour has been observed in numerical solutions of the atmospheric Hadley cell (Held and Hou 1980).

Topographic Hadley cells may be important in continental shelf and slope seas where surface cooling or evaporation drive convective overturning. Over a shelf region with typical parameters $f = 10^{-4}s^{-1}$, $\bar{H} = 200m$ and $\Delta\sigma = 10^{-3}$, relation (22) predicts cell widths of 20km, while relation (10) gives a maximum jet velocity of $2ms^{-1}$ (neglecting the $O(\Delta x/2x_s)$ term). The cells should be easily distinguishable from surface flows driven by along-shelf density gradients, since these keep the coast to their right in the Northern Hemisphere. We will be attempting to identify topographic Hadley cells in archived field data.

ACKNOWLEDGEMENTS

SAC was supported by a fellowship in ocean modeling from the University Corporation for Atmospheric Research.

REFERENCES

BOUBNOV, B M and GOLITSYN, G S (1986) Experimental study of convective structures in rotating fluids. J.Fluid Mech, 167, 503-531.

CHANDRASEKHAR, S (1961) Hydrodynamic and hydromagnetic stability. Oxford University Press, London.

CHEN, R, FERNANDO, H J S and BOYER, D L (1989) Formation of isolated vortices in a rotating convecting fluid. J.Geophys Res, 94, 18445-18453.

FERNANDO, H J S, CHEN, R and BOYER, D L (1991) Effects of rotation on convective turbulence. J.Fluid Mech, 228, 513-547.

HELD, I M and HOU, A Y (1980) Nonlinear axially symmetric circulations in a nearly inviscid atmosphere. J. Atmos.Sci, 37, 515-533.

NAKAGAWA, Y and FRENZEN, P (1955) A theoretical and experimental study of cellular convection in rotating fluids. Tellus, 7, 1-21.